Output Power Smoothing of Wind Power Plants Using Unified Inter-phase Power Controller Equipped with Super-Capacitor

Hajahmadi, Moahammad Ali ; Gharehpetian, Gevork B. GHAREHPETIAN; Firouzi, Mehdi ; Anvari-Moghaddam, Amjad; Blaabjerg, Frede

Published in:
Journal of Energy Storage

DOI (link to publication from Publisher):
10.1016/j.est.2022.105209

Publication date:
2022

Document Version
Publisher's PDF, also known as Version of record

Journal of Energy Storage 54 (2022) 105209

Contents lists available at ScienceDirect

Journal of Energy Storage

journal homepage: www.elsevier.com/locate/est

Research Papers

Output power smoothing of wind power plants using unified inter-phase power controller equipped with super-capacitor

M.A. Hajahmadi [a], G.B. Gharehpetian [a], M. Firouzi [b,*], Amjad Anvari-Moghaddam [c], F. Blaabjerg [c]

[a] Electrical Engineering Department, Amirkabir University of Technology, Tehran, Iran
[b] Department of Electrical Engineering, Abhar Branch, Islamic Azad University, Abhar, Iran
[c] Department of Energy Technology, Aalborg University, Aalborg, Denmark

ARTICLE INFO

Keywords:
Wind power plants (WPPs)
Energy storage system (ESS)
Unified inter-phase power controller (UIPC)
Super-capacitor (SC)
Output power smoothing
Doubly-fed induction generator (DFIG)

ABSTRACT

Due to the growing concerns regarding environmental and economic issues in power systems, nowadays the application of renewable energy sources (RES), especially wind energy has been increased. However, the increasing penetration of wind power plants (WPPs) into the grid has raised numerous challenges including output power fluctuations as well as the significant role these sources play in low-voltage ride-through (LVRT) in case of short circuit fault conditions. Energy storage systems (ESSs) are commonly employed to enhance WPP output power smoothing. On the other side, flexible AC transmission systems (FACTS) can be utilized to enhance dynamic transients of the WPPs under short circuit contingencies. This paper presents the utilization of unified inter-phase power controller (UIPC) and the super-capacitor to fulfill the aforementioned challenges in connection of WPPs to the grid. To achieve this, a novel power control scheme is proposed to compensate for output power variations. The WPP model studied here is of doubly-fed induction generator (DFIG) type wind turbine. Simulations and comparisons are performed in the MATLAB/Simulink® environment to demonstrate the effectiveness of the proposed scheme in smoothening WPP output power as well as enhancing their LVRT capability.

1. Introduction

Nowadays, wind energy has developed far enough to become a worldwide considerable energy resource [1]. Numerous reports highlight that many countries around the globe have already set targets to meet an extensive amount of their electricity demand through wind power by 2030. For instance, the US Department of Energy and the European Wind Energy Association have set goals of 20 % and 22 %, respectively [2]. Wind energy is an inexhaustible and pollution-free renewable energy source (RES), however, the stochastic nature of this RES causes WPPs output power fluctuations, which introduces issues as follows [3–5]:

- Output power variations might lead to fluctuations in power system frequency, especially in weak isolated grids.
- Wind speed variations contribute to output power fluctuations of WPPs as well as their reactive power, which in turn may result in voltage flicker in the power system.

Both aforementioned consequences degrade the overall power quality of the system and may cause instability issues as well, especially to sensitive loads. In the literature, several solutions have been proposed to smooth the fluctuations of WPPs output power, which can be classified into two main categories according to the presence of ESS [6]. One solution is to utilize the energy stored within the wind generation system, including control of the kinetic energy [7,8], pitch angle [9,10], and DC link capacitor voltage [11]. Another alternative is to use ESSs such as superconducting magnetic energy storage (SMES) [12,13], super-capacitor (SC) [14,15], flywheel [16], and various types of batteries [17–19] in WPPs.

The ESS-based power smoothing techniques have similar algorithms. There are two schemes for the installation of ESSs in WPPs; one is to

* Corresponding author.
E-mail addresses: mymahaos@aut.ac.ir (M.A. Hajahmadi), grptian@aut.ac.ir (G.B. Gharehpetian), m.firouzi@abhariau.ac.ir (M. Firouzi), aam@et.aau.dk (A. Anvari-Moghaddam), fbl@et.aau.dk (F. Blaabjerg).

https://doi.org/10.1016/j.est.2022.105209
Received 25 January 2022; Received in revised form 29 May 2022; Accepted 24 June 2022
Available online 26 July 2022

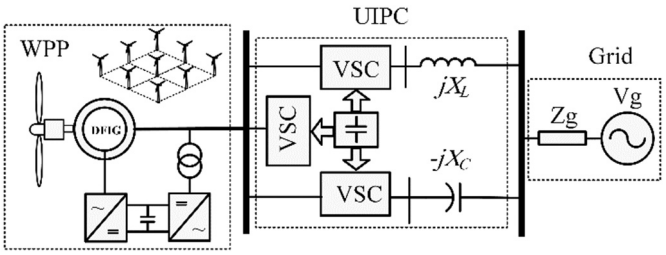

Fig. 1. Wind power plant connected to the power system through UIPC.

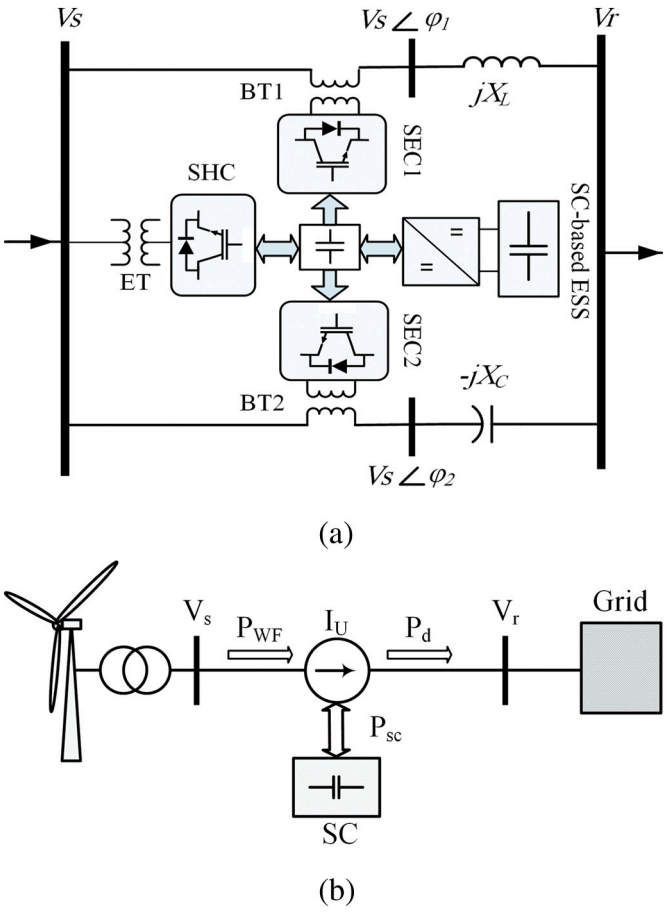

Fig. 2. Schematic diagram of (a) UIPC/ESS power circuit, (b) grid-connected WPP with UIPC/ESS.

connect the ESS to the terminals of the WPP. This scheme requires a voltage source inverter (VSI), a step-down transformer, a buck-boost converter, and a capacitor in DC link which increases the total costs of the system. Another scheme is to connect the ESS to the DC-link of the flexible AC transmission system (FACTS) controllers such as static synchronous compensator (STATCOM) [20,21], unified power flow controller (UPFC) [22], and static synchronous series compensator (SSSC) [23,24], which requires only a buck-boost converter. However, neither of the aforementioned devices can fully isolate WPP from the rest of the grid.

In [25], utilization of UIPC is proposed to connect WPPs to the power system, to control the WPPs output power as well as to limit the contribution of WPPs in fault currents, as depicted in Fig. 1. The UIPC configuration is based on the inter-phase power controller (IPC) [26,27]. However, the phase-shifting transformers in IPC are replaced by three voltage source converters (VSCs), which share a common capacitor in their DC side. UIPC is capable of controlling power flow continuously under steady-state operation and limiting short circuit currents through voltage isolation under fault conditions [28]. In [29], a modified UIPC has been developed for power flow control in a hybrid AC-DC microgrid. In [30], a robust control based on the Quasi Luenberger Observer method has been designed and added to the DC link control of UIPC for power flow control in hybrid microgrids. In [31], a damping controller has been designed and integrated into the UIPC control system to enhance the transient stability of the power system in presence of WPPs. Authors of [32] have utilized UIPC to improve the LVRT capability of WPP. It was recognized as an effective solution to overcome WPPs connection issues. In all of the aforementioned studies, the wind speed is considered constant, and no control scheme has been proposed for variable wind speed WPPs. This is while output power fluctuations caused by variable wind speed are intrinsic to WPPs.

Considering the literature, this paper presents an output power smoothing scheme incorporating a UIPC and SC as storage. The UIPC equipped with ESS can control the power flow and provide a smooth power profile under variable wind speed. Moreover, integrating the ESS increases the UIPC capability to enhance the LVRT performance of WPPs. To achieve this, a novel supervisory control is designed to generate the outer control loop for the UIPC power regulation, as well as the ESS control based on compensating the deviations between WPP output power and its reference value. Simulations are performed in MATLAB/Simulink® environment on a DFIG-based WPP to evaluate the effectiveness of the proposed UIPC/ESS scheme.

The rest of this paper is organized as follows. In Section 2, the structure of the proposed scheme including UIPC and super-capacitor as well as the control system is introduced and elaborated in detail. The next section contains further details regarding super-capacitor ESS and its converter interface to the UIPC. Section 4 includes DFIG-based wind turbine modeling and simulation parameters. The simulation results and discussions are presented in Section 5, in which two main functions of the proposed scheme are separately discussed. Finally, Section 6 concludes the paper.

2. UIPC equipped with ESS

Fig. 2(a) demonstrates the configuration of the UIPC/ESS, which is comprised of two shunt branches; inductive and capacitive. The inductive branch consists of a series inductor and series VSC (SEC1). Similarly, the capacitive branch consists of a series capacitor and series VSC (SEC2). Additionally, a shunt VSC (SHC) is used to provide SEC1 and SEC2 with the required active power. To smoothen the WPP output power, an SC is incorporated in the DC link as ESS. The UIPC is modeled as a voltage-controlled current source I_U, which can be expressed by the following equation [25]:

$$I_U = \frac{V_S}{X}\,\text{sinsin}\,(\alpha)\angle\beta \tag{1}$$

where, $\alpha = (\varphi_2 - \varphi_1)/2$, $\beta = (\varphi_2 + \varphi_1)/2$ and $X = X_L = X_C$. The UIPC active and reactive powers are written by [25]:

$$P_U = 2\frac{|V_s||V_r|}{X}\,\text{sinsin}\,(\alpha)\,\text{coscos}\,(\delta+\beta) \tag{2}$$

$$Q_U = 2\frac{|V_s||V_r|}{X}\,\text{sinsin}\,(\alpha)\,\text{sinsin}\,(\delta+\beta) \tag{3}$$

From Eqs. (2) and (3), the following can be derived.

$$S_U = \sqrt{{P_U}^2 + {Q_U}^2} = 2\frac{|V_s||V_r|}{X}\,\text{sinsin}\,(\alpha) \tag{4}$$

$$\frac{Q_U}{P_U} = \text{tantan}\,(\delta+\beta) \tag{5}$$

Eqs. (4) and (5) are used to obtain α and β for each set of active and reactive power [25,29,30].

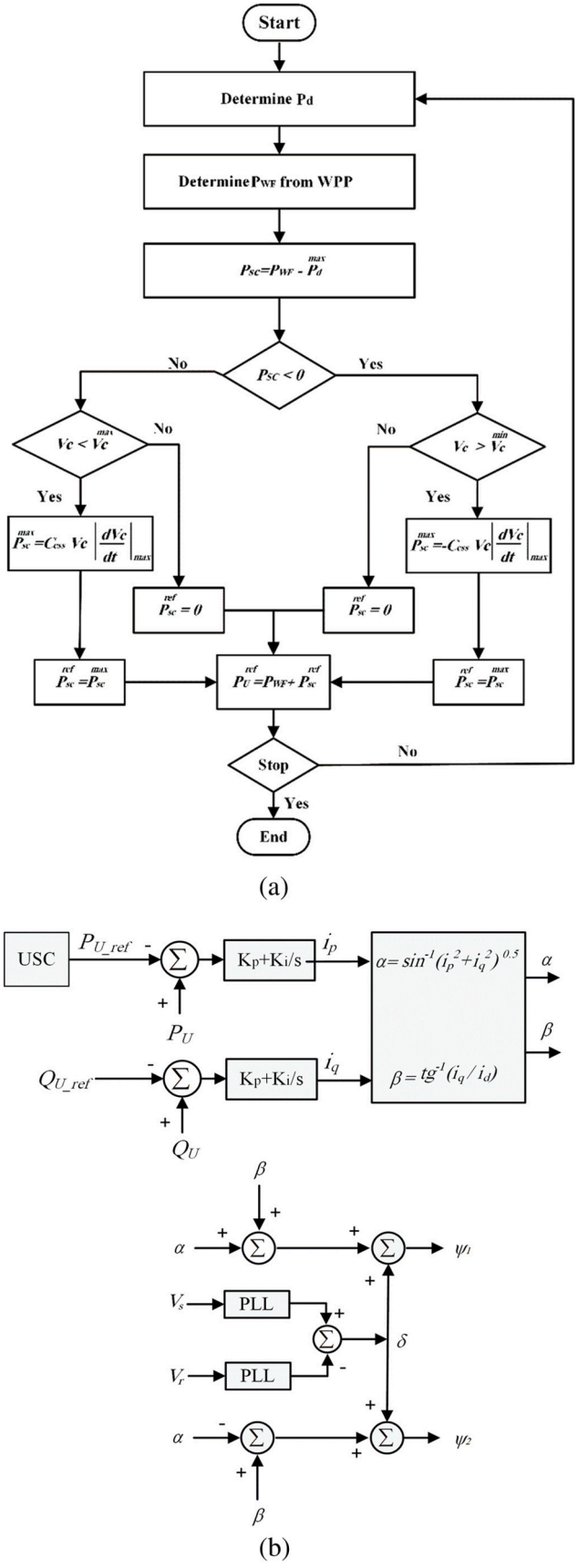

Fig. 3. (a) Flowchart diagram of USC and, (b) UIPC control system.

Fig. 2(b) demonstrates the grid-connected WPP with the UIPC/ESS. The ESS consists of an SC and a bidirectional DC-DC buck/boost converter connected to the UIPC capacitor in its DC link. For the purpose of smoothening WPP power, if the ESS is applied to the WPP, it requires to be integrated at each DFIG DC link, hence making the control strategy of each DFIG and ESS complicated. Considering this problem and to simplify the smooth power control of WPPs, an SC-based ESS is incorporated into the DC link of the UIPC. Using the UPIC/ESS, all wind turbines can operate within their maximum power point, without any modifications to the control system. Moreover, using the ESS enhances the power system transient conditions [21,22].

The ESS contributes to controlling the UIPC active power according to the reference value under variable wind speed. In Fig. 2 (b), P_{WF}, P_d, and P_{sc} represent the WPP output power, output power reference, and active power exchange between the UIPC and ESS systems, respectively. The main function of the UIPC/ESS is to control the WPP output active power according to output power reference (P_d). To achieve this, a UIPC supervisory control (USC) is designed to generate the outer-loop power controllers for the UIPC and ESS control. The flowchart diagram depicted in Fig. 3(a) describes the USC.

To supply the output power reference, the difference between P_d and P_{WF} is injected or stored in the SC as follows:

$$P_{SC} = P_{WF} - P_d \tag{6}$$

On the other hand, the SC voltage (V_C) must satisfy the following inequality constraints:

$$V_C^{min} < V_C < V_C^{max} \tag{7}$$

where, V_C^{max} and V_C^{min} represent the maximum and minimum limits of the SC voltage, respectively. P_{SC}^{max} is the maximum power exchanged between the SC and the UIPC DC link and is determined by:

$$P_{SC}^{max} = \pm C_{ess} V_C \left|\frac{dV_C}{dt}\right|_{max} \tag{8}$$

where, $\left|\frac{dV_C}{dt}\right|_{max}$ is the maximum rate of voltage variations of SC, and

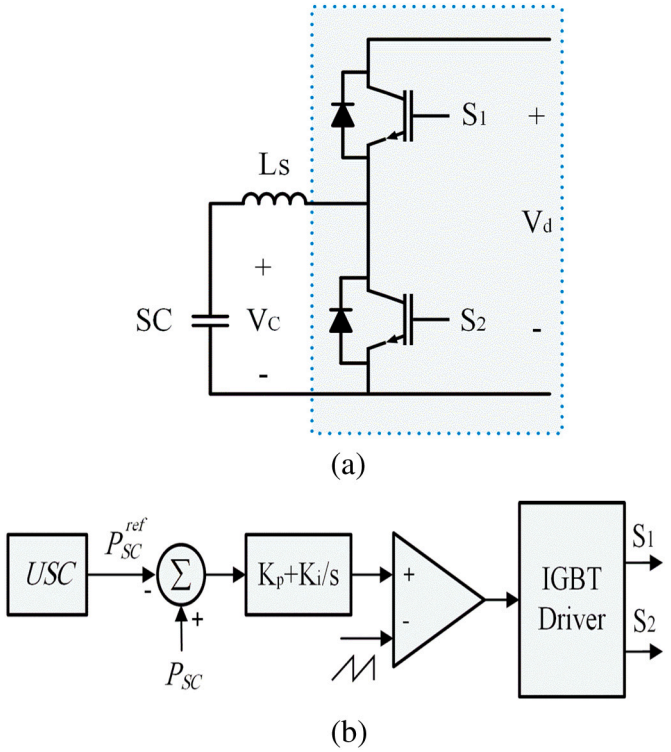

Fig. 4. Configuration of SC-based ESS (a) power circuit, (b) control system.

Table 1
Operation modes of the DC-DC converter.

Condition	S_1	S_2	Operation mode
$P_{ess}^{ref} < 0$	Open	D_2	Boost
$P_{ess}^{ref} > 0$	D_1	Open	Buck

depends on the SC current limit. The positive and negative signs in Eq. (8) denote storing and supplying energy by the SC, respectively. Considering Fig. 3(a), the P_{SC}^{ref} is subjected to V_C^{max} and V_C^{min}. If $P_{SC} > 0$, the SC charges by the DC link capacitor. In this case, if $V_C < V_C^{max}$, P_{SC}^{ref} is calculated using Eq. (8), else $P_{SC}^{ref} = 0$, and the SC cannot store any power. Similarly, if $P_{SC} < 0$, the SC discharges by the DC link capacitor. In this case, if $V_C > V_C^{min}$, P_{SC}^{ref} is calculated using Eq. (8), else $P_{SC}^{ref} = 0$. By calculating P_{SC}^{ref}, the active power reference of the UIPC (P_U^{ref}) is determined as follows:

$$P_U^{ref} = P_{WF} + P_{SC}^{ref} \tag{9}$$

Fig. 3(b) presents the control system of UIPC according to the USC and Eqs. (4) and (5). The control system of the SHC system has been presented in [29–31].

3. SC-based ESS

The SC is an electrochemical capacitor that has a higher energy capacity compared to conventional capacitors. This is due to the employment of conducting polymers as the electrodes, thin dielectric, and large surface area.

The capacitance of the SC is expressed as follows [33]:

$$C_{ess} = \frac{2P_C^{max}T_C}{V_C^2} \tag{10}$$

where P_C^{max}, T_C and V_C represent the maximum stored active power, the period for charging/discharging with P_C^{max}, and the rated SC voltage, respectively.

Fig. 4 demonstrates the control system for switches S_1 and S_2 of the DC/DC converter to regulate the ESS output power. However, it must be noted, to meet the voltage withstand requirements of the semiconductor switching devices, multi-level modular (MMC) topologies are utilized for the bidirectional converter [34]. Considering P_{sc}^{ref} provided by the USC, the DC/DC converter operation is classified into two modes as presented in Table 1. If $P_{WF} < P_d$ (i.e. $P_{sc}^{ref} < 0$), the control system opens S_1 and the DC/DC converter operates in boost mode. In this mode, the SC supplies the active power to the UIPC DC link. If the $P_{WF} > P_d$ (i.e. $P_{sc}^{ref} > 0$), the control system opens S_2 and the DC/DC converter operates in buck mode and the SC absorbs the active power from the DC link.

4. Description of the WPP model

The WPP simulated in this study is modeled by an equivalent aggregated DFIG, derived by an aggregated variable speed WT [35]. The two-mass model drive train is considered in this study to investigate the LVRT response of the DFIG-based WPP [36]. Fig. 5 demonstrates the single line diagram of the study WPP connected to the grid through the UIPC/ESS. The simulated WPP consists of 60 × 1.67 MW DFIG-based WTs. Here, the ESS is designed to absorb/inject 15 % of the UIPC rated power (100 MVA) for 20s. Simulations are performed to demonstrate the UIPC/ESS capability for smoothing output power under variable speed conditions. The power reference is assumed to be 85 MW. Parameters of the UIPC and the system under study are presented in Table 2.

Table 2
Simulation parameters.

Parameter	Value
DFIG	
Rated power	1.67 MW
Number of blades	3
Inertia constant	1.432 s
Stator voltage	0.69 kV
Rotor voltage	2 kV
Nominal frequency	60 Hz
DC voltage	1150 V
Stator resistance	0.023 Ω
Stator reactance	0.18 Ω
Rotor resistance	0.016 Ω
Rotor reactance	0.16 Ω
Capacitor	5 mF
UIPC	
Rated SEC1 and 2	50 MVA
AC voltage	230 kV
DC link voltage	40 kV
$X_L = X_C$	120 Ω
ESS capacitor	60 F
ESS voltage	4 kV
Test system	
Source voltage	230 kV
Nominal power	100 MVA
Line resistance	0.025 Ω/km
Line inductance	0.93 mH/km
Line capacitance	0.012 μF/km

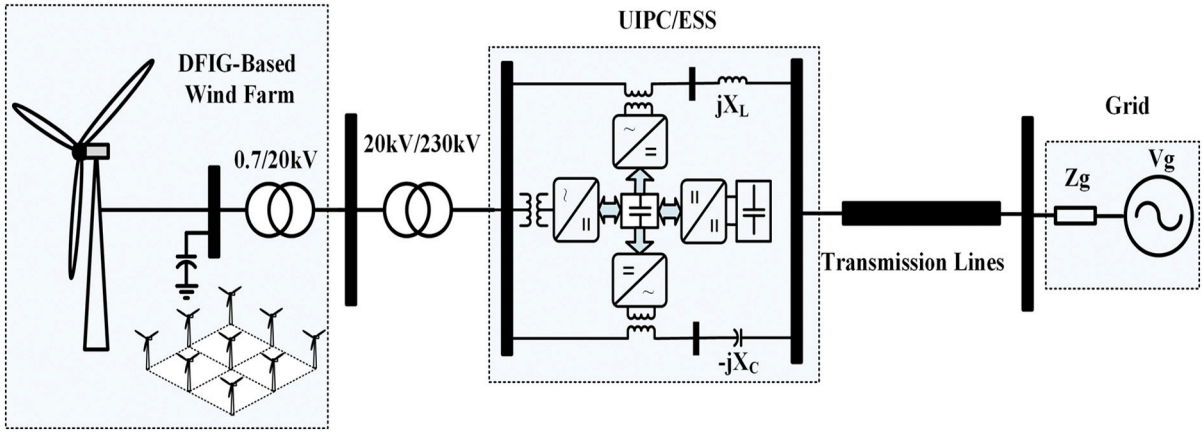

Fig. 5. Single line diagram of the study system with the UIPC/ESS.

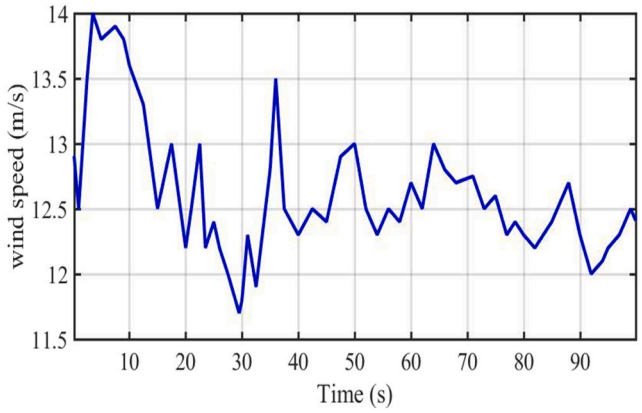

Fig. 6. Wind speed profile.

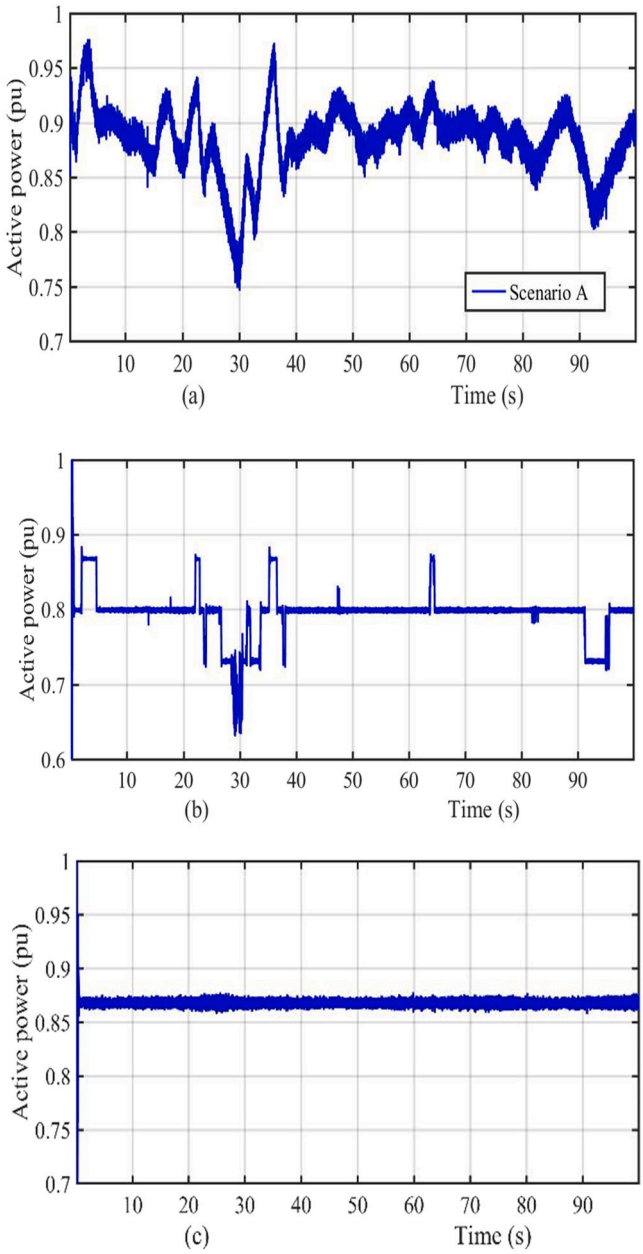

Fig. 7. WPP output power for three scenarios under variable wind speed conditions (a) Scenario A, (b) Scenario B, and, (c) Scenario C.

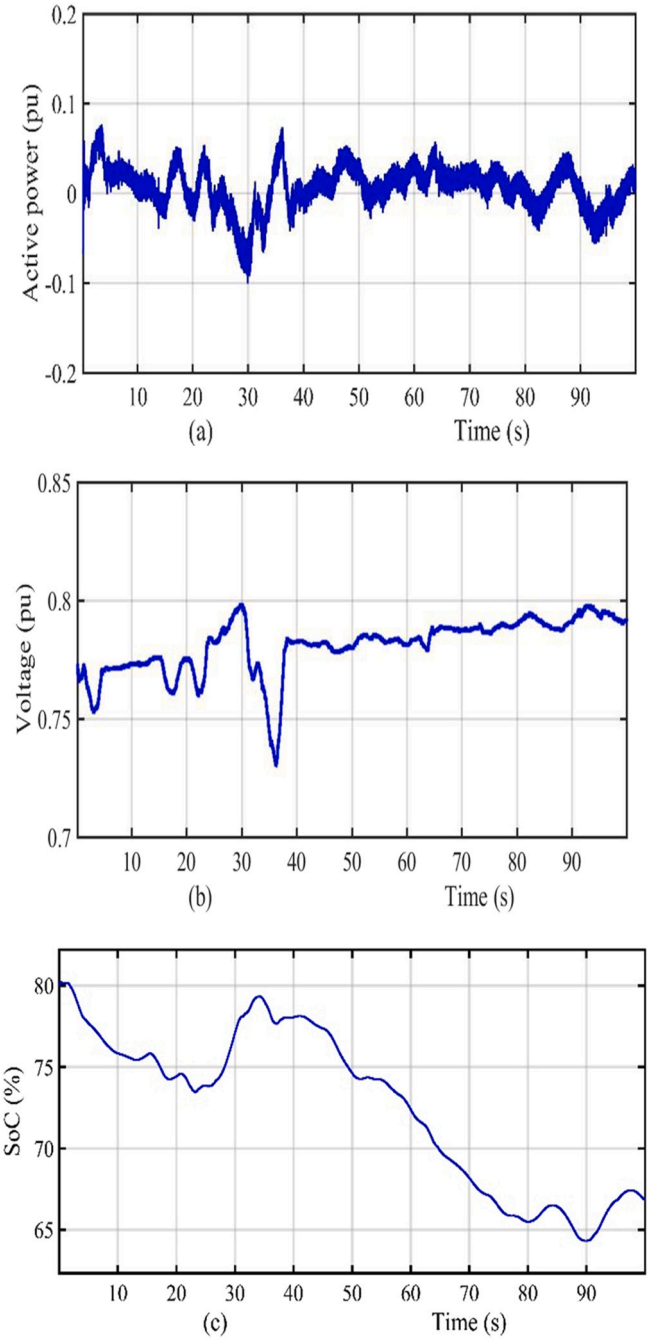

Fig. 8. Super-capacitor (a) output power, (b) voltage, and (c) SOC.

5. Simulation

To investigate the Efficiency of the UIPC/ESS the system shown in Fig. 5 is considered. Firstly, the output power smoothing capability of the WPP is examined using the UIPC/ESS. Afterward, a three-line to ground (3LG) fault is simulated to investigate the LVRT capability of the UIPC/ESS. The following scenarios have been considered:

- Scenario A: Without using any UIPC
- Scenario B: Using the UIPC
- Scenario C: Using the UIPC/ESS.

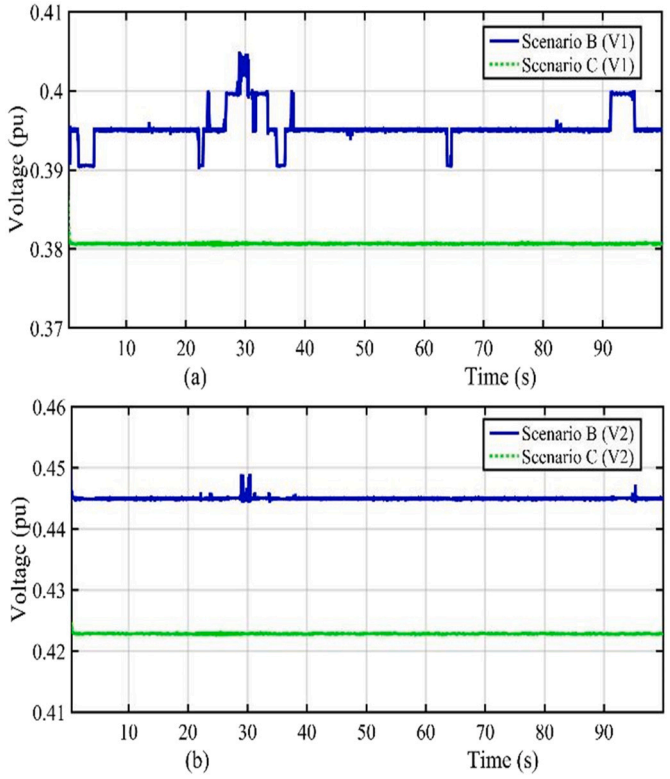

Fig. 9. Voltage injected by (a) inductive SEC branch and, (b) capacitive SEC branch.

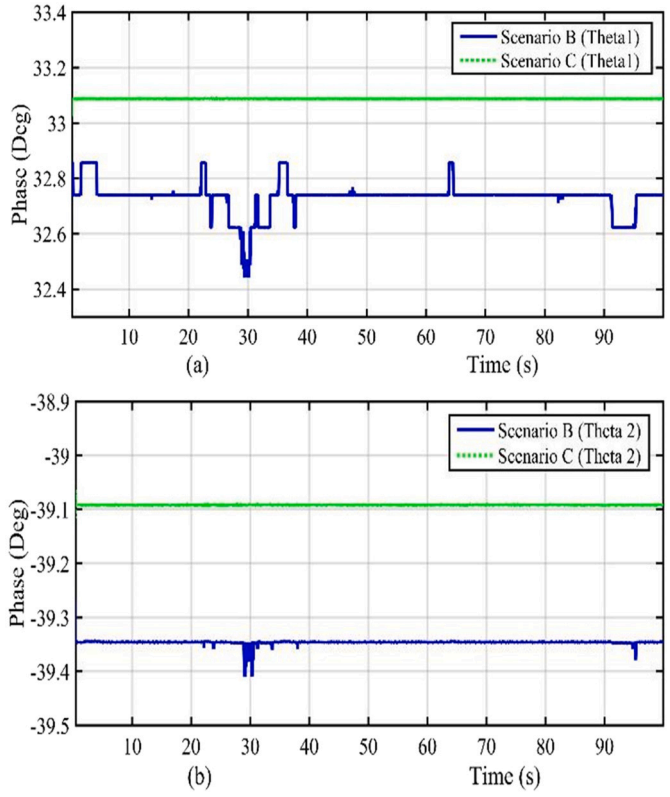

Fig. 10. Voltage phase angle (a) inductive branch and, (b) capacitive branch.

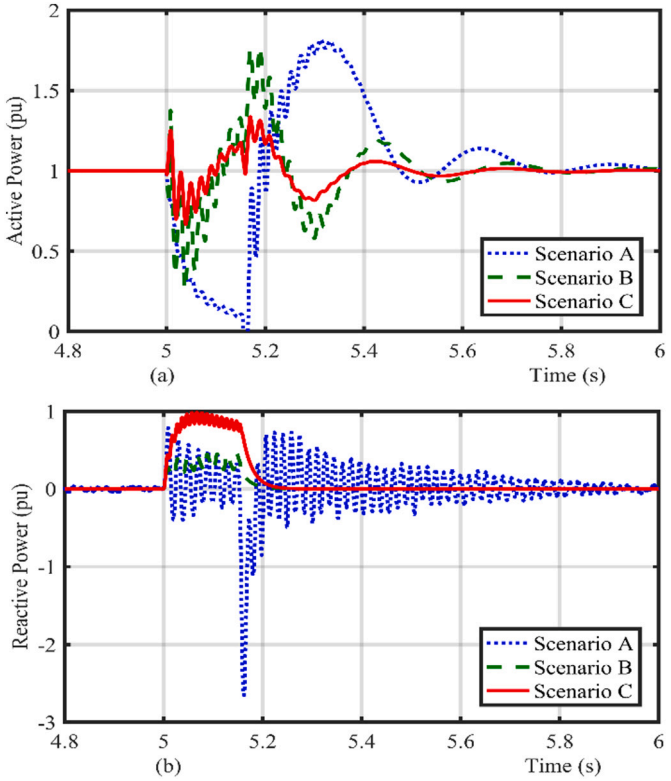

Fig. 11. UIPC/ESS performance under 3LG fault, (a) active power, and (b) reactive power.

5.1. Smoothing output power

In this section, the simulation time is considered to be 100 s to investigate the UIPC/ESS performance under variable wind speed conditions and for all three aforementioned scenarios:

Fig. 6 demonstrates the assumed and simulated wind speed profile, varying from 11.7 m/s to 14 m/s. Fig. 7 demonstrates the WPP output power for three scenarios. In scenario A, the WPP output power fluctuates in the range of 0.75–0.97 pu, as shown in Fig. 7(a). Using the UIPC in scenario B, the WPP output power fluctuations are reduced in the range of 0.7–0.88 pu as shown in Fig. 7(b). However, by using the UIPC/ESS in scenario C, the WPP output power is controlled at 0.87 pu according to power reference as shown in Fig. 7(c).

Fig. 8(a) and (b) demonstrates the output active power and voltage of super-capacitor ESS under variable speed, respectively. When the wind power generation is more than the calculated reference, the ESS stores extra power and vice versa as shown in Fig. 8(a). Fig. 8(c) shows the super-capacitor state of charge (SOC) of super-capacitor under variable speed. Fig. 9(a) and (b) depicts the inductive and capacitive SECs injected voltage to control the WPP output power for scenarios B and C, according to the power reference. It can be observed from this figure that the inductive and capacitive SEC voltages are controlled in 0.38pu and 0.423pu in scenario C, respectively. However, they are varied according to wind speed variations in the case of using UIPC in scenario B. Fig. 10 (a) and (b) shows the inductive and capacitive branches voltage phase angles to control the WPP output power for scenarios B and C. In scenario B, the phase angle of the inductive branch varies in the range of 32.5 to 32.8 degrees. However, it is controlled at 33.1 degrees in scenario C.

5.2. Enhancing LVRT capability

In this section, a 3LG fault is simulated on the transmission line to evaluate the capability of the UIPC/ESS for enhancing the LVRT

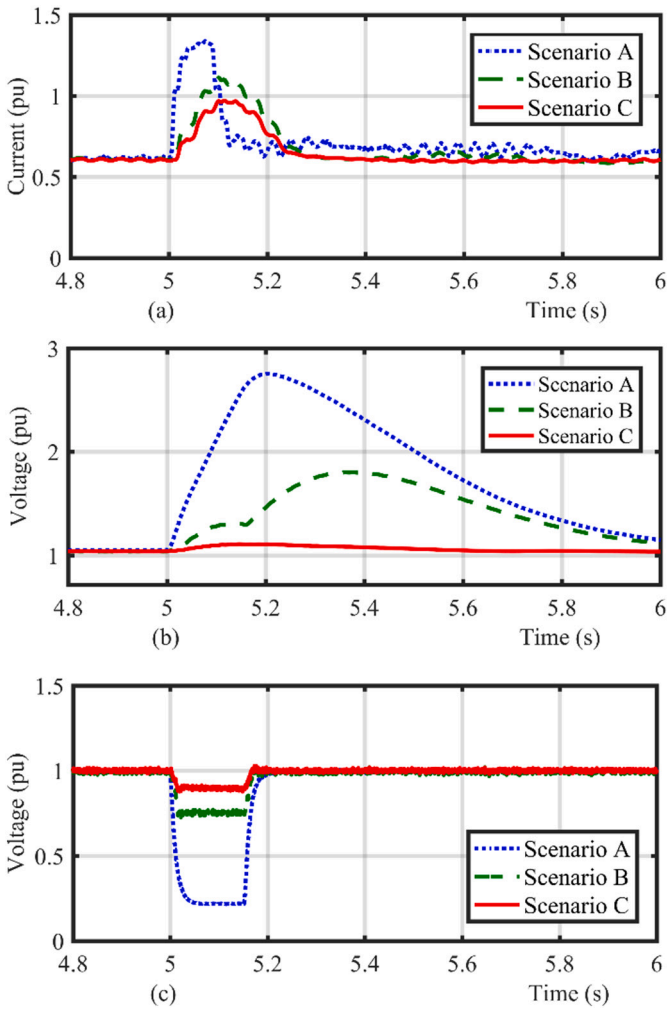

Fig. 12. UIPC/ESS performance under 3LG fault, (a) rotor current, (b) DC link voltage, (c) terminal voltage.

capability of WPP. The fault occurs at $t = 5$ s and lasts for 150 ms. Wind speed is considered to be 15 m/s and constant. Fig. 11(a) shows the active power of the WPP under this condition for all scenarios. In scenario A, the WPP active power drops to zero, approximately. In scenario B, the WPP active power reduces to 0.5 pu at fault instant and raises to 1.6 pu after fault clearance.

However, by using the UIPC/ESS in scenario C, it has lower oscillation and power drop compared with scenario B. Fig. 11(b) shows the reactive power in this condition for all scenarios.

It can be seen from this figure that the WPP absorbs −2.6 pu reactive power from the grid in scenario A. However, in scenarios B and C, the UIPC injects 0.5 and 0.9 pu reactive power to enhance the LVRT capability of the WPP, respectively.

Fig. 12(a) shows the rms value of rotor current for all scenarios. As shown in this figure, the rotor current raises to 1.3 pu in scenario A. However, in the other two scenarios, the rotor current is effectively limited to 1.2 pu and 0.95 pu, respectively. Fig. 12(b) shows the DC link voltage for all scenarios. It can be seen that by using the UIPC/ESS, the DC link voltage remains constant during the fault period. Fig. 12(c) shows the WPP terminal voltage for all scenarios. In scenario A, the terminal voltage falls to 0.2 pu. However, the terminal voltage is 0.8pu and 0.92pu for scenarios B and C under this condition.

6. Conclusion

In this paper is presented an output power smoothing scheme for WPPs, based on UIPC equipped with SC-based ESS. To achieve this, a supervisory control has been designed to generate the reference power for the UIPC and ESS. Additionally, its performance is compared to the case of utilizing UIPC without ESS under variable wind speed in normal and 3LG fault conditions.

Simulation results demonstrate that using the UIPC/ESS, the output power of WPP is effectively smoothened. Moreover, integration of the ESS to the UIPC increases the UIPC capability to enhance the LVRT performance of WPP.

CRediT authorship contribution statement

M. A. Hajahmadi: Investigation, Methodology, Software, Validation
G. B. Gharehpetian: Investigation, Supervision
M. Firouzi: Conceptualization, Writing- Original draft preparation
Anvari. Moghadam: Supervision, Writing- Reviewing and Editing
F. Blaabjerg: Supervision.

Declaration of competing interest

The authors declare that they have no conflict of interest.

References

[1] G. W. E. Council, Global Wind 2015 Report: Annual Market Update, Global Wind Energy Council (GWEC), Brussels, Belgium, 2016.
[2] L. Qu, W. Qiao, Constant power control of DFIG wind turbines with supercapacitor energy storage, IEEE Trans. Ind. Appl. 47 (1) (2011) 359–367.
[3] X Lyu, J. Zhao, Y. Jia, Zh. Xu, K.P. Wong, Coordinated control strategies of PMSG-Based wind turbine for smoothing power fluctuations, IEEE Trans. Power Syst 34 (1) (2019) 391–401.
[4] T. Ikegami, C.T. Urabe, T. Saitou, K. Ogimoto, Numerical definitions of wind power output fluctuations for power system operations, Renew. Energy 115 (2018) 6–15.
[5] F. Jia, X. Cai, Z. Li, Frequency-distinct control of wind energy conversion system featuring smooth and productive power output, IEEE Access 6 (2018) 16746–16754.
[6] A.M. Howlader, N. Urasaki, A. Yona, T. Senjyu, A.Y. Saber, A review of output power smoothing methods for wind energy conversion systems, Renew. Sust. Energ. Rev. 26 (Oct. 2013) 135–146.
[7] S.G. Varzaneh, G. Gharehpetian, M. Abedi, Output power smoothing of variable speed wind farms using rotor-inertia, Electr. Power Syst. Res. 116 (2014) 208–217.
[8] Y. Zhu, Y. Guo, Zh. Wang, Zh. Wei, Kinetic energy based output power smoothing control and parameters design for PMSG-WECSs, Int. J. Electr. Power Energy Syst. 131 (Oct 2021) 107077, https://doi.org/10.1016/j.ijepes.2021.107077.
[9] M. Chowdhury, N. Hosseinzadeh, W. Shen, Fuzzy logic systems for pitch angle controller for smoothing wind power fluctuations during below rated wind incidents, in: PowerTech, 2011 IEEE Trondheim, IEEE, 2011, pp. 1–7.
[10] M. Chowdhury, N. Hosseinzadeh, W. Shen, Smoothing wind power fluctuations by fuzzy logic pitch angle controller, Renew. Energy 38 (1) (2012) 224–233.
[11] A. Uehara, et al., A coordinated control method to smooth wind power fluctuations of a PMSG-based WECS, IEEE Trans. Energy Convers. 26 (2) (2011) 550–558.
[12] J.X. Jin, R.H. Yang, R.T. Zhang, Y.J. Fan, Q. Xie, X.Y. Chen, Combined low voltage ride through and power smoothing control for DFIG/PMSG hybrid wind energy conversion system employing a SMES-based AC-DC unified power quality conditioner, Int. J. Electr. Power Energy Syst. 128 (June 2021) 106733.
[13] M. Sheikh, S. Muyeen, R. Takahashi, J. Tamura, Smoothing control of wind generator output fluctuations by PWM voltage source converter and chopper controlled SMES, Eur. Trans. Electr. Power 21 (1) (2011) 680–697.
[14] M. Kenan Döşoğlu, A.B. Arsoy, Transient modeling and analysis of a DFIG based wind farm with supercapacitor energy storage, Int. J. Electr. Power Energy Syst. 78 (June 2016) 414–421.
[15] C. Abbey, G. Joos, Supercapacitor energy storage for wind energy applications, IEEE Trans. Ind. Appl. 43 (3) (2007) 769–776.
[16] R. Cárdenas, R. Peña, G. Asher, J. Clare, Power smoothing in wind generation systems using a sensorless vector controlled induction machine driving a flywheel, IEEE Trans. Energy Convers. 19 (1) (2004) 206–216.
[17] M. Khalid, A. Savkin, A model predictive control approach to the problem of wind power smoothing with controlled battery storage, Renew. Energy 35 (7) (2010) 1520–1526.
[18] M.T. Zareifard, A.V. Savkin, Model predictive control for wind power generation smoothing with controlled battery storage, in: 2015 10th Asian Control Conference (ASCC) 2015 10th Asian Control Conference (ASCC), IEEE, Kota Kinabalu, Malaysia, September 2015.
[19] S. Teleke, M.E. Baran, A.Q. Huang, S. Bhattacharya, L. Anderson, Control strategies for battery energy storage for wind farm dispatching, IEEE Trans. Energy Convers. 24 (3) (2009) 725–732.
[20] M. Beza, M. Bongiorno, An adaptive power oscillation damping controller by STATCOM with energy storage, IEEE Trans. Power Syst. 30 (1) (2015) 484–493.

[21] A. Kanchanaharuthai, V. Chankong, K.A. Loparo, Transient stability and voltage regulation in multimachine power systems vis-à-vis STATCOM and battery energy storage, IEEE Trans. Power Syst. 30 (5) (2015) 2404–2416.
[22] Q. Wang, S. Choi, The design of battery energy storage system in a unified power-flow control scheme, IEEE Trans. Power Deliv. 23 (2) (2008) 1015–1024.
[23] A. Bidadfar, et al., Power swings damping improvement by control of UPFC and SMES based on direct Lyapunov method application, in: IEEE Power and Energy Society General Meeting, 2008, pp. 1–7.
[24] T. Mahto, V. Mukherjee, Frequency stabilisation of a hybrid two-area power system by a novel quasi-oppositional harmony search algorithm, IET Gener. Transm. Distrib. 9 (15) (Nov. 2015) 2167–2179.
[25] M. Firouzi, G.B. Gharehpetian, B. Mozafari, Power-flow control and short-circuit current limitation of wind farms using unified interphase power controller, IEEE Trans. Power Deliv. 32 (1) (2017) 62–71.
[26] J. Brochu, F. Beauregard, J. Lemay, G. Morin, P. Pelletier, R. Thallam, Application of the interphase power controller technology for transmission line power flow control, IEEE Trans. Power Deliv. 12 (2) (1997) 888–894.
[27] M. Farmad, S. Farhangi, G.B. Gharehpetian, S. Afsharnia, Nonlinear controller design for IPC using feedback linearization method, Int. J. Electr. Power Energy Syst. 44 (1) (Jan 2013) 778–785, https://doi.org/10.1016/j.ijepes.2012.08.036.
[28] J. Pourhossein, G. Gharehpetian, S. Fathi, Unified interphase power controller (UIPC) modeling and its comparison with IPC and UPFC, IEEE Trans. Power Deliv. 27 (4) (2012) 1956–1963.
[29] M. Zolfaghari, M. Abedi, G.B. Gharehpetian, Power flow control of interconnected AC-DC microgrids in grid-connected hybrid microgrids using modified UIPC, IEEE Trans. Smart Grid, IEEE Trans. Energy Convers. 10 (6) (Nov. 2019) 6298–6307.
[30] Mahdi Zolfaghari, G.B. Gharehpetian, A. Anvari-Moghaddam, Quasi-Luenberger observer-based robust DC link control of UIPC for flexible power exchange control in hybrid microgrids, IEEE Syst. J. 15 (2) (June 2021) 2845–2854.
[31] M. Firouzi, G.B. Gharehpetian, S.B. Mozafari, Application of UIPC to improve power system stability and LVRT capability of SCIG-based wind farms, IET Gener. Transm. Distrib. 11 (9) (2017) 2314–2322.
[32] M. Firouzi, G.B. Gharehpetian, Y. Salami, Active and reactive power control of wind farm for enhancement transient stability of multi-machine power system using UIPC, IET Renew. Power Gener. 11 (8) (2017) 1246–1252.
[33] Y. Errami, M. Ouassaid, M. Maaroufi, Optimal power control strategy of maximizing wind energy tracking and different operating conditions for permanent magnet synchronous generator wind farm, Energy Procedia 74 (2015) 477–490.
[34] N. Flourentzou, V.G. Agelidis, G.D. Demetriades, VSC-based HVDC power transmission systems: an overview, IEEE Trans. Power Electron. 24 (3) (2009) 592–602.
[35] L. Fernandez, C. Garcia, F. Jurado, Equivalent model of wind farms by using aggregated wind turbines and equivalent winds, Energy Covers. Manag. 50 (2009) 691–704.
[36] M. Firouzi, G.B. Gharehpetian, LVRT performance enhancement of DFIG-based wind farms by capacitive bridge-type fault current limiter, IEEE Trans. Energy Convers. 9 (3) (2018) 1118–1125.